ACS Catalysis

Research Article

pubs.acs.org/acscatalysis

Mechanisms of the Deactivation of SAPO-34 Materials with Different Crystal Sizes Applied as MTO Catalysts

Weili Dai,[†] Guangjun Wu,[†] Landong Li,*[,†] Naijia Guan,[†] and Michael Hunger*[,‡]

[†]Key Laboratory of Advanced Energy Materials Chemistry (Ministry of Education), College of Chemistry, Nankai University, Tianjin 300071, People's Republic China

[‡]Institute of Chemical Technology, University of Stuttgart, 70550 Stuttgart, Germany

Supporting Information

ABSTRACT: SAPO-34 materials with comparable Brønsted acid site density but different crystal sizes were applied as methanol-to-olefin (MTO) catalysts to elucidate the effect of the crystal size on their deactivation behaviors. ^{13}C HPDEC MAS NMR, FTIR, and UV/vis spectroscopy were employed to monitor the formation and nature of organic deposits, and the densities of accessible Brønsted acid sites and active hydrocarbon-pool species were studied as a function of time-on-stream (TOS) by ^{1}H MAS NMR spectroscopy. The above-mentioned spectroscopic methods gave a very complex picture of the deactivation mechanism consisting of a number of different steps. The most important of these steps is the formation of alkyl aromatics with large alkyl chains improving at first the olefin selectivity, but hindering the reactant diffusion after longer TOS. The hindered reactant diffusion leads to a surplus of retarded olefinic reaction products in the SAPO-34 pores accompanied by their oligomerization and the formation of polycyclic aromatics. Finally, these polycyclic aromatics are responsible for a total blocking of the SAPO-34 pores, making all catalytically active sites inside the pores nonaccessible for further reactants.

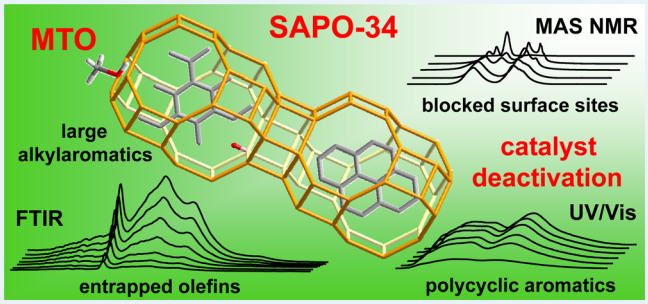

KEYWORDS: *methanol-to-olefin conversion, SAPO-34, crystal size, deactivation mechanism, Brønsted acid sites, benzene-based carbenium ions, in situ spectroscopy*

1. INTRODUCTION

As an alternative process for obtaining olefins, methanol-to-olefin (MTO) conversion on microporous solid acid catalysts has attracted extensive attention since it was disclosed in the 1970s.[1−5] During recent decades, a variety of molecular sieves have been explored as possible MTO catalysts,[6−17] and it is generally acknowledged that the MTO performances of molecular sieves are controlled both by their framework structure and by their acidity.[2] The silicoaluminophosphate molecular sieve SAPO-34 with Brønsted acid sites of moderate acid strength and a well-defined framework with chabazite cages connected via 8-ring windows is reported to be the most promising catalyst, giving a maximum light olefin (propene and ethene) yield of ∼80%.[1,2] The catalytic and mechanistic aspects of the MTO reaction on SAPO-34 have been extensively studied (for an overview, see refs 3−5). According to the well accepted hydrocarbon pool mechanism, polyalkyl aromatics confined inside the cages of SAPO-34 are active reaction intermediates leading to the formation of light olefins upon activation by Brønsted acid sites at the framework. The small 8-ring windows of ∼3.8 Å restrict the diffusion of heavy and branched hydrocarbons and, therefore, lead to a high selectivity to the desired light olefins.

A key problem of SAPO-34 for its application as an industrial MTO catalyst is the rapid deactivation of this material.[18−21] For clarifying the reasons of the deactivation, extensive attention has been paid to controlling the Brønsted acidity of SAPO-34 to obtain a highly active catalyst with a long lifetime.[6,7,22−25] In addition to the acidity, the crystal size of SAPO-34 is also an important factor that may influence the catalytic performance, especially the catalyst lifetime in the MTO, reaction due to coke formation. SAPO-34 with small crystal size has been reported to exhibit a prolonged lifetime in MTO conversion due to its good resistance to deactivation by coke.[26−30] However, to the best of our knowledge, detailed spectroscopic investigations on the deactivation mechanisms of SAPO-34 catalysts in the MTO process in relation to dependence on the crystal size and the Brønsted acidity have been missing until now and are, therefore, the goal of the present work.

In this study, SAPO-34 materials with different crystal sizes were synthesized and characterized by means of XRD, SEM, and solid-state NMR spectroscopy. The MTO performances of these materials were evaluated in a fixed-bed reactor, and the organic intermediates formed during MTO reaction were analyzed by in situ FTIR and UV/vis spectroscopy. Specifically, the dynamic changes in the Brønsted acid sites and benzene-

Received: January 3, 2013
Revised: February 18, 2013
Published: February 20, 2013

   dx.doi.org/10.1021/cs400007v | ACS Catal. 2013, 3, 588−596

type carbenium ions during the MTO reaction were monitored by ^{1}H solid-state NMR spectroscopy using ammonia-loaded catalyst samples. On the basis of the catalytic and spectroscopic results, the deactivation behavior of SAPO-34 with different crystal sizes in the MTO reaction are revealed, and the deactivation mechanisms of these catalysts are discussed.

2. EXPERIMENTAL SECTION

2.1. Preparation and Characterization of the SAPO-34 Catalysts. The SAPO-34 catalysts were synthesized by a hydrothermal method using the structure-directing agents TEAOH (tetraethylammonium), TriEA (triethylamine), and MOR (morpholine) following the procedures described in the literature.[29,31,32] The chemical compositions of the synthesis mixtures and the conditions for the synthesis of different SAPO-34 samples are summarized in Table 1. Ortho phosphoric acid solution (85 wt %) and aluminumtriisopropylate (ATI) were mixed with distilled water and stirred for 2 h, followed by dropwise addition of the structure-directing agents and silica sol (neutral, 30 wt %, Alfa Aesar). The mixture was further stirred for 6 h at room temperature, and the formed gel was transferred into a Teflon-lined stainless-steel autoclave for static crystallization. After crystallization at the temperatures and with the durations given in Table 1 (columns 3 and 4), the solid products were separated by a centrifuge, washed four times with demineralized water, and dried at 353 K for 12 h. The as-synthesized samples were then calcined in flowing synthetic air at 873 K for 6 h.

Table 1. Synthesis Parameters of the SAPO-34 Materials under Study with Different Crystal Sizes

sample	batch composition[a]	temp/K	time/h	ref
SAPO-34-S	$1Al_2O_3/1P_2O_5/0.6SiO_2/0.5TEAOH/77H_2O$	473	24	29
SAPO-34-M	$1Al_2O_3/1P_2O_5/0.6SiO_2/2TriEA/50H_2O$	473	24	31
SAPO-34-L	$1A1_2O_3/1P_2O_5/0.6SiO_2/2MOR/60H_2O$	463	48	32

[a]Molar ratios.

X-ray diffraction (XRD) patterns of the calcined samples were recorded on a Bruker D8 diffractometer with Cu Kα radiation (λ = 1.5418 Å) at 5−50° with a scan rate of 2θ = 6.0°/min.

A JEOL-JSM7500 field emission scanning electron microscope (FESEM) was used to study the crystal morphologies. The SEM images were recorded after covering the samples with a thin layer of gold, deposited by sputtering.

The chemical compositions of the calcined samples were determined by inductively coupled plasma atomic emission spectrometer (ICP-AES, IRIS Advantage). The surface areas of the calcined SAPO-34 materials were obtained by means of nitrogen adsorption at 77 K on a Quantachrome Autosorb 3B instrument. Before the nitrogen adsorption, the samples were dehydrated at 473 K for 2 h. The total surface areas were calculated via the Brunauer−Emmett−Teller (BET) equation.

Solid-state NMR investigations of the catalyst framework were performed with hydrated samples on a Bruker Avance III 400WB spectrometer at resonance frequencies of 104.3, 79.5, and 161.9 MHz for ^{27}Al, ^{29}Si, and ^{31}P nuclei, respectively. The MAS spectra were recorded upon single pulse excitation of $\pi/6$ for ^{27}Al and $\pi/2$ for ^{29}Si and ^{31}P, with repetition times of 0.5 s for ^{27}Al, 20 s for ^{29}Si, and 30 s for ^{31}P and sample spinning rates of 8 kHz for ^{27}Al and ^{31}P nuclei, and a rate of 4 kHz was used for the study of ^{29}Si nuclei. To avoid hydrolysis of framework bonds, the hydration of the samples was performed not longer than 1 day before the NMR characterization by exposing them to an atmosphere saturated with the vapor of an aqueous solution of $Ca(NO_3)_2$ at ambient temperature.

2.2. MTO Reaction over the SAPO-34 Catalysts. The MTO reaction was investigated in a fixed-bed reactor at atmospheric pressure. Typically, 0.4 g of the SAPO-34 catalysts (sieve fraction, 0.25−0.5 mm) was placed in a stainless steel reactor (5 mm i.d.) and activated under flowing nitrogen gas at 723 K for 1 h. After cooling to the reaction temperature of 673 K, ^{12}C-methanol or ^{13}C-enriched methanol (see section 2.3.) was injected at a rate of 0.5 mL/h, corresponding to the weight hourly space velocity of WHSV = 1.0 h^{-1}. The products were analyzed by an online gas chromatograph, HP5890/II, with flame ionization detector and a packed-column Porapak Q to separate the C_1−C_8 hydrocarbons. The temperature of the column was maintained at 313 K for 15 min and then increased to 473 K at a heating rate of 10 K/min. The methanol conversions and the selectivities to the various reaction products for different times on stream were calculated without considering the coke contents of the catalysts, which was exclusively determined at the end of the catalytic experiments.

2.3. Characterization of Entrapped Organic Compounds on the Used SAPO-34 Catalysts. The nature of organic compounds formed on the catalysts during the MTO reaction was in situ monitored by FTIR and UV/vis spectroscopy. FTIR spectra were recorded in the diffuse reflection mode on a Bruker Tensor 27 spectrometer equipped with a high sensitivity MCT detector cooled by liquid nitrogen and an in situ reaction chamber. Prior to the FTIR studies, ∼20 mg of the catalyst materials was finely ground and placed in the chamber. The samples were activated in flowing helium gas at 723 K for 1 h and cooled to 673 K for taking a background spectrum. Then, methanol was injected into the reaction chamber at a flow rate of 0.025 mL/h (WHSV = 1.0 h^{-1}), and time-resolved spectra were recorded with a resolution of 4 cm^{-1} and an accumulation of 128 scans. The UV/vis spectra were recorded in the diffuse reflection mode in the range of 200−600 nm using an AvaSpec-2048 fiber optic spectrometer, an AvaLight-DH-S deuterium light source by Avantes, and a glass fiber reflection probe HPSUV1000A by Oxford Electronics. Before starting the MTO reaction, the glass fiber reflection probe was placed in the fixed-bed reactor on the top of the catalyst with a gap of ∼1.0 mm to the catalyst bed. Reference UV/vis spectra of the catalysts were recorded at reaction temperature prior to starting the methanol flow.

The organic deposits entrapped inside the pores and cages of SAPO-34 were characterized by ^{13}C HPDEC MAS NMR spectroscopy on a Bruker Avance III 400WB spectrometer at a resonance frequency of 100.6 MHz, with $\pi/2$ pulse excitation, a repetition time of 20 s, a sample spinning rate of 12.0 kHz, and high-power proton decoupling (HPDEC). ^{13}C-enriched methanol (99%, Cambridge Isotope Laboratories, Inc., USA), mixed with nonenriched methanol at a ratio of 1:1, was used for performing the MTO reaction in a standard fixed-bed reactor before taking samples of the SAPO-34 catalysts after times on-stream of TOS = 30 min to 1 h. For this purpose, the MTO reaction was quenched by stopping the methanol flow at reaction temperature and cooling down within 1 h under nitrogen flow (60 mL/min). Subsequently, all catalyst samples studied by NMR spectroscopy were transferred from the fixed-

dx.doi.org/10.1021/cs400007v | ACS Catal. 2013, 3, 588−596

bed reactor into gastight MAS NMR rotors inside a glovebox purged with dry nitrogen gas to avoid contact with air.

The amounts of entrapped organic compounds after the MTO reaction were analyzed by thermogravimetric analysis (TGA) on a Setram Setsys 16/18 thermogravmetric analyzer. In a typical measurement, 0.1 g of the used catalyst materials was heated in an Al_2O_3 crucible at a constant heating rate of 10 K/min under flowing synthetic air of 30 mL/min.

2.4. ^{1}H MAS NMR Characterization of Surface Sites and Benzene-Based Carbenium Species. The Brønsted acid sites of the fresh and used SAPO-34 samples were characterized by means of ^{1}H MAS NMR spectroscopy utilizing a Bruker Avance III 400WB spectrometer at a resonance frequency of 400.1 MHz, with $\pi/2$ single pulse excitation, a repetition time of 10 s, and a sample spinning rate of 25.0 kHz using a 2.5 mm MAS NMR probe. Before the ^{1}H MAS NMR studies of the fresh SAPO-34 catalysts, these materials were dehydrated at 673 K in vacuum (pressure below 10^{-2} Pa) for 12 h. Subsequently, the materials were sealed and kept in glass tubes until their transfer into MAS NMR rotors inside a glovebox purged with dry nitrogen gas. The used SAPO-34 catalysts were obtained after stopping the MTO reaction and transferring them into MAS NMR rotors without contact to air. The determination of the number of accessible Brønsted acid sites was performed upon adsorption of ammonia at room temperature and by evaluating the ^{1}H MAS NMR signals caused by ammonium ions (δ_{1H} = 6.5−7.0 ppm). For this purpose, the catalyst samples were loaded with 100 mbar ammonia and, subsequently, evacuated at 453 K for 2 h to eliminate physisorbed ammonia. Quantitative ^{1}H MAS NMR measurements were performed by comparing the signal intensities of the samples under study with the intensity of an external intensity standard (dehydrated zeolite H,Na−Y with a cation exchange degree of 35%). The chemical shift values were referenced to tetramethylsilane. The decomposition and simulation of NMR spectra were carried out via the Bruker software WINFIT.

3. RESULTS AND DISCUSSION

3.1. Physicochemical Properties of the SAPO-34 Catalysts. The XRD patterns of the as-synthesized materials shown in Figure 1 are typical for the chabazite (CHA) framework structure,[33] which indicates that pure SAPO-34 catalysts were obtained. In Figure 2, the FESEM images of the crystal morphologies of the as-synthesized SAPO-34 materials are shown. All three SAPO-34 materials consist of crystals with a cubical shape, whereas their crystal sizes are quite different. On the basis of their crystal sizes, the samples are assigned SAPO-34-S (small: 2.5 μm), SAPO-34-M (medium: 6.0 μm), and SAPO-34-L (large: 20.0 μm). The chemical compositions and BET surface areas of the calcined SAPO-34 materials under study are given in Table 2. The $n_{Si}/(n_{Si} + n_{Al} + n_P)$ ratios and surface areas of all three SAPO-34 materials are very similar and occur in the ranges of 0.11−0.12 and 441−471 m^2/g, respectively, indicating that the crystal size is exclusively the deviating parameter.

For a better understanding of the textual properties of SAPO-34 after calcination, ^{29}Si, ^{31}P, and ^{27}Al MAS NMR spectroscopy (see Figure S1 in the Supporting Information) was employed to investigate the local structure of the framework silicon, phosphorus, and aluminum atoms, respectively, in the SAPO-34 samples under study. The ^{29}Si MAS NMR spectra with signals occurring exclusively at −92 to −89 ppm indicate the presence of tetrahedrally coordinated framework silicon atoms with four aluminum atoms in the next-nearest coordination sphere of T atoms ($Si(OAl)_4$) and the absence of silicon islands.[34,35] The domination signal of the ^{31}P MAS NMR spectra appearing at −28 ppm hints at tetrahedrally coordinated phosphorus atoms in the aluminophosphate framework.[35] In the ^{27}Al MAS NMR spectra, strong signals were observed at 30−44 ppm, which are caused by tetrahedrally coordinated framework aluminum atoms, whereas the much weaker signals at −14 to −11 ppm are due to octahedrally coordinated aluminum atoms formed by coordination of two additional water molecules to tetrahedrally coordinated framework aluminum atoms or by extraframework aluminum species.[36] On the basis of the results of the solid-state NMR characterization, it could be concluded that the local structures of the framework atoms in all three SAPO-34 materials are very similar and maintained the textual properties of intact silicoaluminophosphates after their calcination.

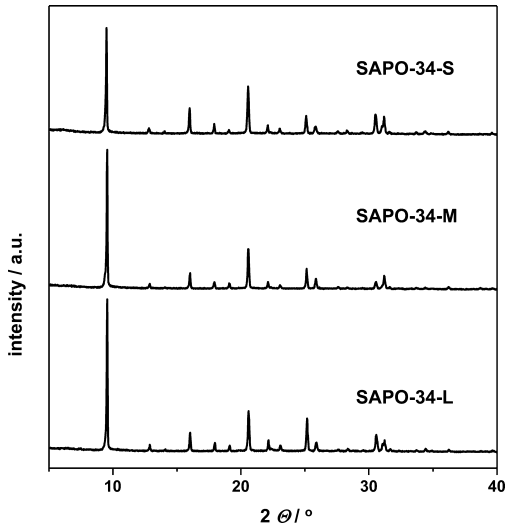

Figure 1. XRD patterns of the as-synthesized SAPO-34-S (top), SAPO-34-M (middle), and SAPO-34-L (bottom) materials.

3.2. Catalytic Performances of the SAPO-34 Catalysts in the MTO Reaction. In Figure 3, the methanol conversion and product selectivity curves of the SAPO-34 catalysts in the MTO reaction are shown. It is obvious that the crystal size has a great impact on the lifetime of the MTO catalysts under study. For SAPO-34-S, a methanol conversion of 100% and a selectivity to light olefins of more than 90% were obtained at 673 K and maintained for a time-on-stream (TOS) of up to 10 h. After TOS = 10 h, the selectivity to C_2−C_4 olefins gradually decreased and dropped to ∼5% at TOS = 16 h, while the methanol conversion decreased from 100% to ∼75%. For SAPO-34-M, a methanol conversion of 100% and a selectivity to light olefins of ∼90% was maintained only up to TOS = 4 h. After TOS = 10 h, the selectivity to light olefins rapidly decreased to ∼5% while dimethylether (DME) became the dominant product (∼90%). In comparison with SAPO-34-S and SAPO-34-M, the deactivation rate of large-crystalline SAPO-34-L is much more rapid. Typically, 100% methanol conversion could be only maintained for TOS = 10 min. Afterward, the methanol conversion decreased dramatically to 40% after TOS = 30 min.

3.3. TGA Analysis and ^{13}C HPDEC MAS NMR Investigations of Organic Deposits on the Deactivated

dx.doi.org/10.1021/cs400007v | ACS Catal. 2013, 3, 588−596

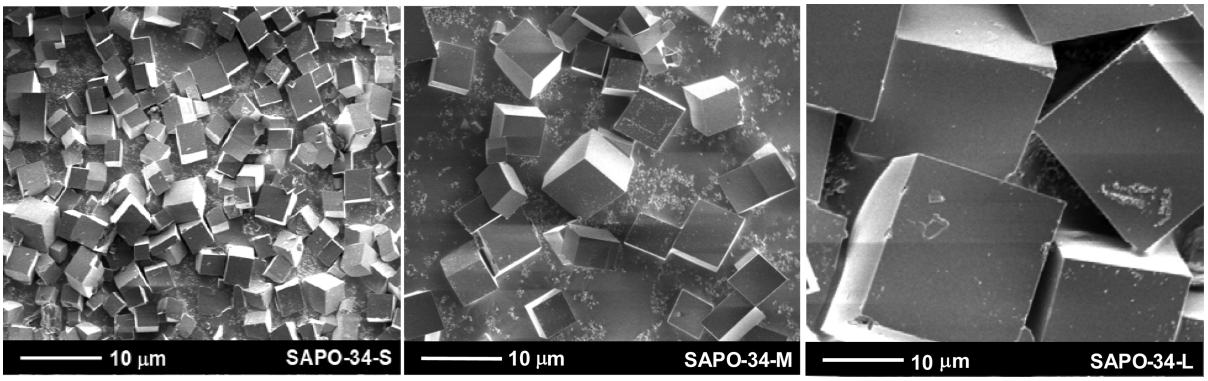

Figure 2. SEM images of the as-synthesized SAPO-34-S (left), SAPO-34-M (middle), and SAPO-34-L (right) materials.

Table 2. Chemical Compositions and Surface Areas of the Calcined SAPO-34 Materials under Study

	elemental analysis[a] (mmol/g)					
sample	n_{Al}	n_P	n_{Si}	$n_{Si}/(n_{Si} + n_{Al} + n_P)$	BET surface area[b] (m^2/g)	Brønsted acid sites[c] (mmol/g)
SAPO-34-S	6.6	4.9	1.5	0.12	441	1.25
SAPO-34-M	6.1	4.6	1.4	0.12	464	1.15
SAPO-34-L	6.0	4.1	1.1	0.11	471	1.00

[a]Determined by ICP-AES. [b]Determined by N_2 absorption [c]Determined by ^{1}H MAS NMR

SAPO-34 Catalysts. The total weights of organic deposits formed on SAPO-34-S, SAPO-34-M, and SAPO-34-L after their deactivation in the MTO reaction were analyzed by TGA in the temperature range of 293−1073 K. According to Figure 4, all samples showed a similar weight loss of ∼1.9 wt % at temperature up to 473 K due to the escape of volatile compounds. In the high-temperature range of 473−1073 K, the weight losses for the deactivated SAPO-34-S (TOS = 16 h), SAPO-34-M (TOS = 16 h), and SAPO-34-L (TOS = 30 min) were 6.0, 11.5, and 9.0 wt %, respectively. Hence, the amount of organic deposits formed on SAPO-34-S during the MTO reaction is obviously lower than that on SAPO-34-M and SAPO-34-L, which should be a very important reason for the prolonged lifetime of SAPO-34-S. The amount of organic deposits formed on SAPO-34-L after TOS = 60 min is only slightly lower than that on SAPO-34-M after TOS = 16 h, indicating the much more rapid accumulation of organic compounds on SAPO-34-L.

The ^{13}C HPDEC MAS NMR spectra of the used SAPO-34 catalysts obtained after the MTO reaction for TOS = 1 h and 30 min are shown in Figure 5. For all samples under study, strong signals of aromatic carbon atoms (125−133 ppm) and alkyl carbon atoms bound to aromatic rings (12−30 ppm) occur.[37] These signals indicate the formation of polyalkyl aromatics as dominant organic species over the SAPO-34 catalysts during the MTO reaction. Interestingly, the number of methylene carbon atoms ($-CH_2-$) in the alkyl groups of polyalkyl aromatics on SAPO-34-S (Figure 5, top), reflected by the signals at 24−30 ppm, is significantly lower than that of SAPO-34-M (Figure 5, middle) at TOS = 1 h and SAPO-34-L (Figure 5, bottom) at TOS = 30 min. On the basis of this observation, it can be concluded that polyalkyl aromatics with long alkyl groups (C_2, C_3, etc. instead of C_1) are more rapidly accumulated on SAPO-34 samples with larger crystal sizes (SAPO-34-M and SAPO-34-L) during MTO reaction and vice versa.

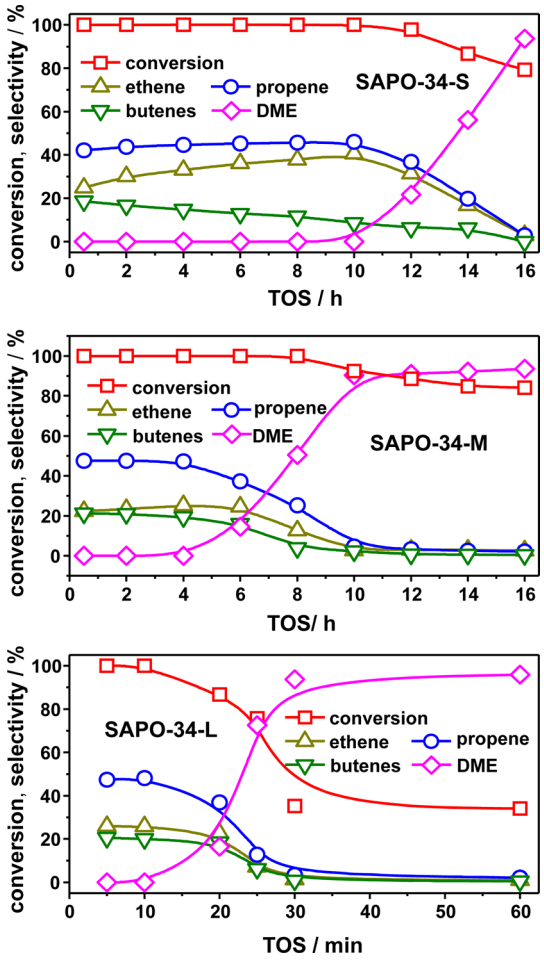

Figure 3. Methanol conversion and product selectivities during the MTO conversion over the SAPO-34 catalysts under study at 673 K.

3.4. In Situ FTIR and UV/Vis Studies of the MTO Reaction over the SAPO-34 Catalysts. In situ FTIR and UV/vis spectroscopy were utilized to investigate the nature of organic compounds formed during the MTO reaction on the catalysts under study. Figure 6 shows the in situ FTIR spectra of the species adsorbed and entrapped on the different SAPO-34 catalysts during the MTO reaction at 673 K and in steps of 30 min. For all three SAPO-34 catalysts under study, strong

dx.doi.org/10.1021/cs400007v | ACS Catal. 2013, 3, 588−596

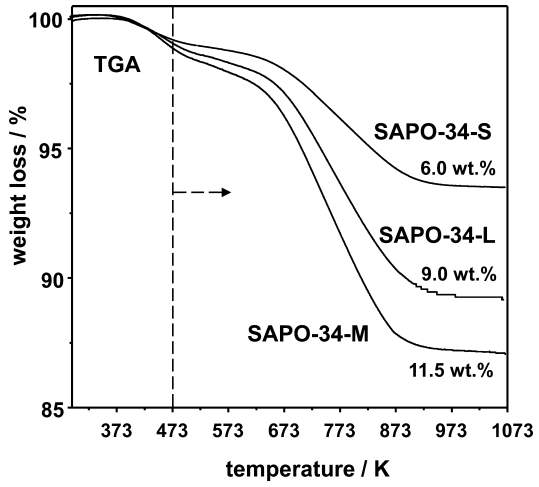

Figure 4. TGA curves of the SAPO-34-S (top), SAPO-34-M (bottom), and SAPO-34-L (middle) materials obtained at 673 K after TOS = 16 h for SAPO-34-S and SAPO-34-M and after TOS = 60 min for SAPO-34-L.

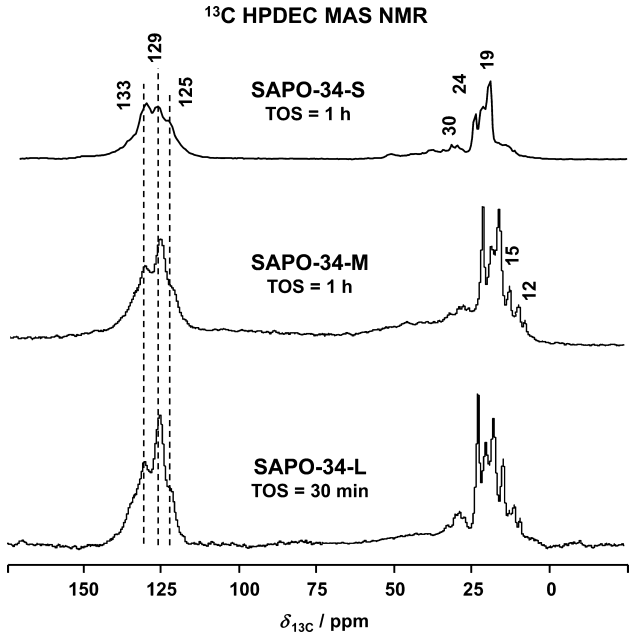

Figure 5. ^{13}C HPDEC MAS NMR spectra of the MTO catalysts under study obtained at 673 K after TOS = 1 h for SAPO-34-S (top) and SAPO-34-M (middle) and after TOS = 30 min for SAPO-34-L (bottom).

bands at 2873−2948 cm^{-1} due to C−H stretching vibrations and weak bands at 1608−1621, 1503, 1461−1463, and 1380 cm^{-1} due to skeletal C═C vibrations of aromatics and the bending vibrations of C−H bond could be observed.[38−41] The intensities of these bands increased with the progress of the MTO reaction. In addition, negative bands at 3610 cm^{-1} due to Brønsted acid sites interacting with adsorbate molecules occurred for all SAPO-34 under study upon starting the MTO reaction (see insets in Figure 6). This indicates that the Brønsted acid sites were gradually covered by methanol or reaction products. Furthermore, with increasing reaction time, two very narrow bands due to the C−H stretching and methyl bending vibrations appeared at 3017 and 1304 cm^{-1}. These bands reached their maximum intensities for the deactivated

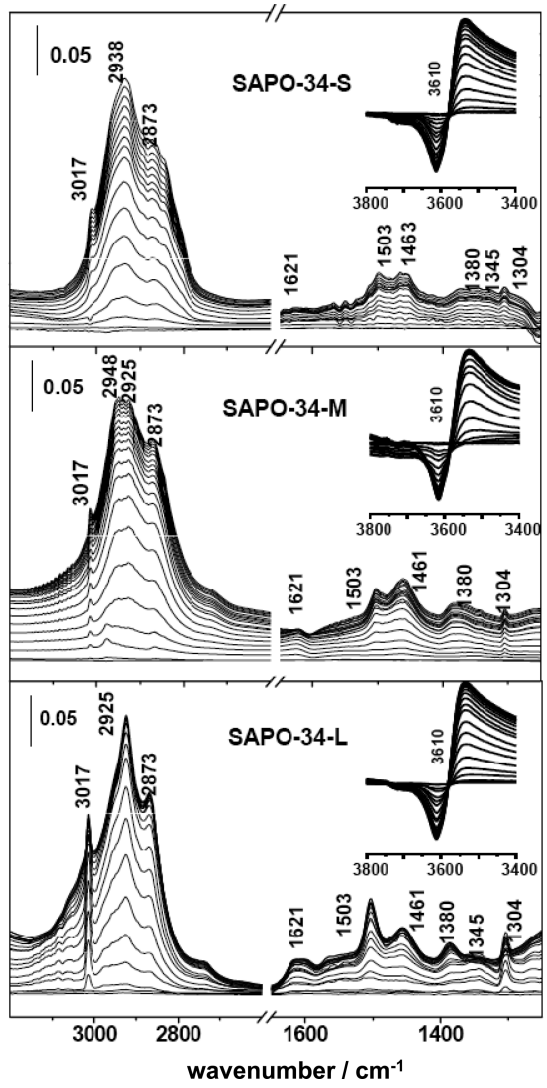

Figure 6. In situ FTIR spectra recorded during the MTO reaction at 673 K over the calcined SAPO-34-S (top), SAPO-34-M (middle), and SAPO 34-L (bottom) catalysts up to TOS = 30 min.

SAPO-34-L. The wavenumber of 3017 cm^{-1} hints at C−H stretching vibrations involving carbon atoms with double bonds (═CH or ═CH$_2$), which are typical for olefins and dienes.[42] Considering this assignment and the small width of the bands at 3017 cm^{-1}, their observation hints at the presence of light olefins with a retarded desorption from the SAPO-34 catalysts with increasing reaction time. The presence of light olefins with long residence time inside the SAPO-34 pores and cages leads to an accelerated formation of oligomerization products, such as aromatics acting as coke deposits, which indicates the end of the catalyst lifetime. Because of the weak integral intensities of the FTIR bands caused by entrapped light olefins with retarded desorption properties, their number is too low for an observation by ^{13}C HPDEC MAS spectroscopy.

In Figure 7, the in situ UV/vis spectra recorded during the MTO reaction over the SAPO-34 catalysts under study at 673 K and with a TOS of up to 30 min are shown. For all three SAPO-34 catalysts, similar organic species were formed during the MTO reaction, leading to a series of UV/vis bands at ∼240, 270, 330, 390−400, and 450−475 nm. During the first 3 min, that is, in the induction period of the MTO reaction, a rapid increase in the UV/vis bands at 240, 270, and 400 nm was

dx.doi.org/10.1021/cs400007v | ACS Catal. 2013, 3, 588−596

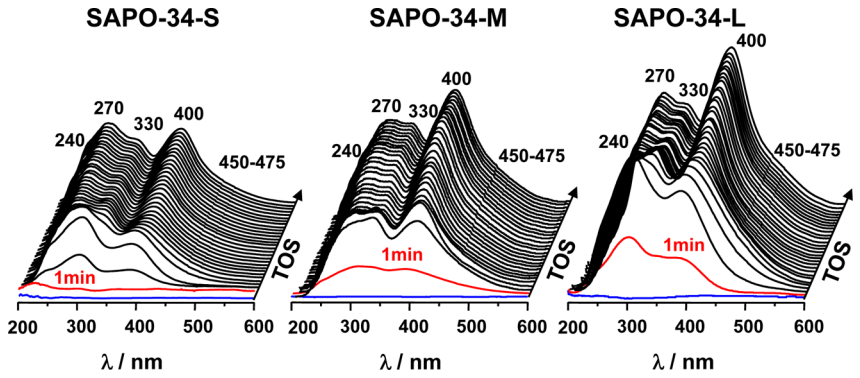

Figure 7. In situ UV/vis spectra recorded during the MTO reaction at 673 K over the calcined SAPO-34-S (left), SAPO-34-M (middle), and SAPO-34-L (right) catalysts up to TOS = 30 min.

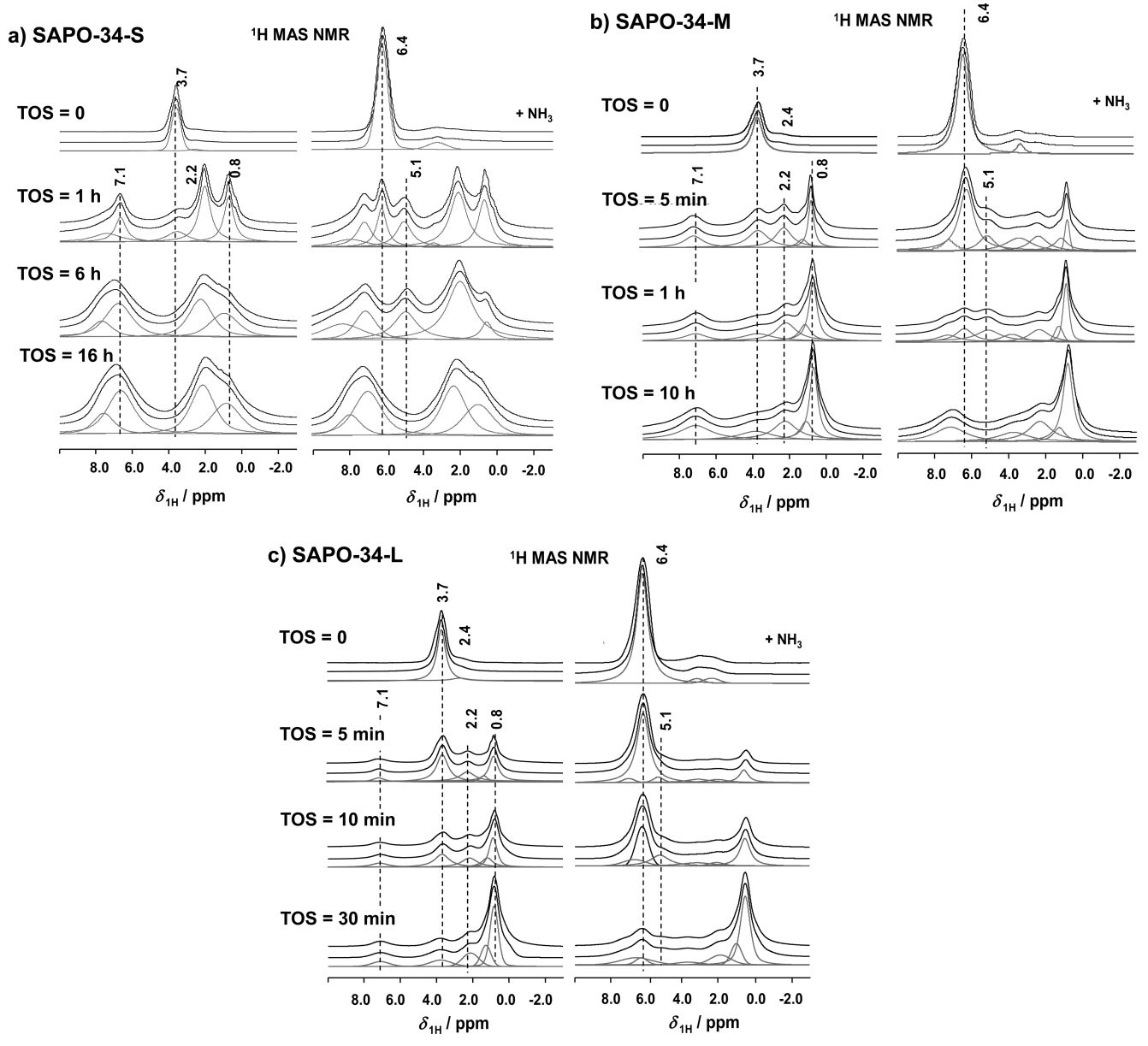

Figure 8. ^{1}H MAS NMR spectra of the MTO catalysts under study obtained at 673 K for TOS up to 16 h in the case of SAPO-34-S (a), up to 10 h in the case of SAPO-34-M (b), and up to 30 min in the case of SAPO-34-L (c).

observed which was due to the formation of initial compounds of the hydrocarbon pool. With further progress of the MTO reaction (TOS > 3 min), additional bands occurred at 330 and 450−475 nm, and the band intensities at ∼400 nm increased.

dx.doi.org/10.1021/cs400007v | ACS Catal. 2013, 3, 588−596

On the basis of earlier UV/vis studies of organic compounds on acidic zeolite catalysts,[12,43−47] the bands at 240 and 270 nm were assigned to UV/vis-sensitive dienes and polyalkyl aromatics, respectively, and bands at 390 nm were explained by benzene-type carbenium ions.[47] Bands at ∼400 nm hint at the formation of polycyclic aromatics,[45,48,49] for example, with two to three condensed aromatic rings at lower wavelengths and with four condensed aromatic rings at slightly higher wavelengths than 400 nm.[50] Broad bands occurring at 330 and 450−475 nm can be due to dienylic and trienylic carbenium ions, respectively.[46] The in situ UV/vis spectra reveal that with increasing time-on-stream and for larger crystal size, the band at 270 nm due to alkyl aromatics becomes dominating in the high-frequency region (see, e.g., Figure 7, right). Simultaneously, the bands at ∼400 nm due to polycyclic aromatics are increasing in the low-frequency region.

A direct comparison of the different SAPO-34 catalysts allows the UV/vis spectra recorded at TOS = 1 min, which are marked in red (Figure 7). These spectra demonstrate that the large-crystalline SAPO-34-L is characterized by a very rapid formation of alkyl aromatics (270 nm). Already at TOS = 10 min, polycyclic aromatics appearing at ∼400 nm dominate the low-frequency region of the UV/vis spectra of SAPO-34-M and SAPO-34-L. These large organic species block the cages and pore entrances of the SAPO-34 catalysts, which leads to a masking of Brønsted acid sites and a retarded desorption of reaction products, both of which accelerate the deactivation, as proved by the strong decrease in the methanol conversion curves in Figure 3.

3.5. ^{1}H MAS NMR Study of the Fate of Brønsted Acid Sites and Carbenium Species during MTO Reaction. To investigate the fate of Brønsted acid sites and active hydrocarbon pool species on SAPO-34 samples, the calcined and used catalyst samples taken from the fixed-bed reactor after different TOS were analyzed by ^{1}H MAS NMR spectroscopy without and after loading of ammonia (Figure 8, left and right, respectively).

The ^{1}H MAS NMR spectrum of calcined SAPO-34-S (TOS = 0) is dominated by a signal at 3.7 ppm, corresponding to bridging OH groups, that is, Brønsted acid sites (Figure 8a, top, left). Adsorption of ammonia on the accessible Brønsted acid site leads to the formation of ammonium ions, causing a ^{1}H MAS NMR signal at 6.4 ppm (Figure 8a, top, right). Evaluation of this ammonium signal gave 1.25 mmol/g accessible Brønsted acid sites in the calcined SAPO-34-S before its catalytic application. After TOS = 1 h, strong signals at 1.0−2.3 and 7.4−8.5 ppm corresponding to hydrogen atoms bound to carbon atoms in saturated and unsaturated compounds,[43] respectively, can be observed in the ^{1}H MAS NMR spectrum recorded before and after ammonia loading. Meanwhile, the intensity of signal at 3.7 ppm corresponding to Brønsted acid site in SAPO-34 strongly decreased. On the basis of the signal intensities in the spectrum of the ammonia-loaded sample, the Brønsted acid site density was calculated to be 0.32 mmol/g. In this spectrum of the ammonium-loaded sample, a new signal at 5.1 ppm assigned to phenylammonium ions occurred,[43] which is caused by the ammoniation of benzene-type carbenium ions. The benzene-type carbenium has been recognized as the key hydrocarbon pool species for MTO reaction using SAPO-34 as catalyst. According to the evaluation results summarized in Table 3, the number of benzene-type carbenium ions in SAPO-34-S increased to a value of 0.69 mmol/g after TOS = 6 h, while the number of accessible Brønsted acid sites decreased to 0 mmol/g. Interestingly, SAPO-34-S still exhibited a good MTO activity at this TOS (compare Figure 3). After deactivation of SAPO-34-S at TOS = 16 h, neither accessible Brønsted acid sites nor benzene-based carbenium ions could be detected (Table 3, last column).

Table 3. Numbers of Accessible Brønsted Acid Sites (SiOHAl groups), n_{SiOHAl}, and Benzene-Based Carbenium Ions, $n_{benzenium}$, on the Calcined and Used SAPO-34 Catalysts under Study as Determined by ^{1}H MAS NMR Spectroscopy for Different Times on Stream (TOS) after Ammonia Adsorption

sample	TOS	n_{SiOHAl}[a] (mmol/g)	$n_{benzenium}$[a] (mmol/g)	$n_{SiOHAl} + n_{benzenium}$ (mmol/g)
SAPO-34-S	0	1.25	0	1.25
	1 h	0.32	0.38	0.70
	6 h	0	0.69	0.69
	16 h	0	0	0
SAPO-34-M	0	1.15	0	1.15
	5 min	0.46	0.15	0.61
	1 h	0.24	0.36	0.60
	10 h	0	0	0
SAPO-34-L	0	1.00	0	1.00
	5 min	0.48	0.09	0.57
	10 min	0.38	0.17	0.55
	30 min	0.02	0	0.02

[a]Determined by ^{1}H MAS NMR after ammonia absorption

According to the spectra in Figure 8b and c and considering the data summarized in Table 3, the SAPO-34-M and SAPO-34-L catalysts showed similar trends in the changes of the number of accessible Brønsted acid sites and benzene-based carbenium ions, such as SAPO-34-S; however, in a significantly accelerated manner. Also for these catalysts, the total consumption of accessible Brønsted acid sites and benzene-based carbenium ions led to their strong deactivation.

The above-mentioned findings agree with the observations in our earlier work focusing on the fate of Brønsted acid sites in SAPO-34 during the MTO process.[43] Upon regeneration of the used SAPO-34 catalysts in synthetic air at 873 K, the ^{1}H MAS NMR signals of bridging OH groups occurred again with nearly the same intensities as observed for the fresh material; hence, the MTO reaction does not lead to a dehydroxylation of SAPO-34 catalysts. But during the MTO reaction, these hydroxyl groups are involved in the formation of adsorbate complexes of different nature (e.g., alkoxy groups, protonation of aromatics, hydrogen bondings to deposits etc.), which is accompanied by a shift and broadening of their ^{1}H MAS NMR signals initially appearing at 3.6 ppm.

3.6. Deactivation Mechanisms of SAPO-34 Materials Applied as MTO Catalysts. The different spectroscopic methods utilized in the present work for investigating the deactivation of SAPO-34 catalysts during the MTO conversion gave a very complex picture. This picture consists of a number of elements obtained by in situ UV/vis, FTIR, and solid-state NMR spectroscopy being complementary methods, sensitive for very different aspects of the deactivation process.

Considering the Brønsted acidity as a key property of SAPO-34 materials for their application as MTO catalysts, ^{1}H MAS NMR spectroscopy has shown that all three SAPO-34 materials under study—SAPO-34-S, SAPO-34-M, and SAPO-34-L—have a similar number of accessible Brønsted acid sites before starting the MTO reaction. However, the number of accessible

dx.doi.org/10.1021/cs400007v | ACS Catal. 2013, 3, 588−596

Brønsted acid sites decreased after a short reaction time, especially for the large-crystalline SAPO-34-L material. Interestingly, before the strong deactivation of the SAPO-34 catalysts occurred, no accessible Brønsted acid sites could be detected by ^{1}H MAS NMR spectroscopy. On the other hand, although the number of accessible Brønsted acid sites decreased, the number of benzene-based carbenium ions increased during the highly active reaction period of the SAPO-34 catalysts. The above-mentioned observation indicates that benzene-based carbenium ions play a key role as catalytically active hydrocarbon pool compounds in the MTO conversion over SAPO-34. This statement is supported by the absence of accessible benzene-type carbenium species in the strongly deactivated SAPO-34 catalysts.

As demonstrated by UV/vis spectroscopy, the reaction period characteristic of the formation of benzene-type formation is the same as that of the formation of alkyl aromatics in general (UV/vis band at 270 nm). In the case of the large-crystalline SAPO-34-L material, ^{13}C HPDEC MAS NMR spectroscopy indicated that these alkyl aromatics have longer alkyl chains consisting of more methylene carbon atoms (^{13}C HPDEC MAS NMR signals at 24−30 ppm) on the used SAPO-34-L and SAPO-34-M catalysts in comparison with those formed on SAPO-34-S. At first, these larger alkyl aromatics may have the advantage of increasing the selectivity to ethene. After longer time-on-stream, however, the increasing organic deposits influence and hinder the reactant diffusion, which was also demonstrated in our recently published PFG NMR study on reactant diffusion in SAPO-34 used as MTO catalysts.[44]

Simultaneous with first indications of a catalyst deactivation, narrow bands of olefinic species (FTIR bands at 3017 cm^{-1}) occurred in the FTIR spectra. Their observation by FTIR spectroscopy hints at an enhanced residence time of these reaction products in the SAPO-34 cages and pores, which may be caused by their retarded desorption due to large alkyl aromatics. Because of the high reactivity of the olefinic reaction products, a surplus of these species in the SAPO-34 cages and pores is accompanied by their rapid oligomerization, such as the formation of polycyclic aromatics, as indicated by UV/vis spectroscopy (UV/vis bands at ∼400 nm). Finally, these polycyclic aromatics cause a total blocking of the SAPO-34 pores, which strongly hinders the diffusion of reaction products and makes all catalytically active sites and species nonaccessible for further reactants. Since especially the latter deactivation steps are accompanied by a hindering of the reactant diffusion, the total decrease in the olefin formation over the large-crystalline SAPO-34-L occurred after a significantly shorter MTO reaction time and is much more rapid than that observed for SAPO-34-S and SAPO-34-M, with significantly smaller crystal sizes. Furthermore, the accelerated blocking of cage pores in the large-crystalline SAPO-34-L material is the reason for the lower total coke formation in SAPO-34-L in comparison with SAPO-34-S (see TGA data). In the case of SAPO-34-L, the pores and cages of the outer sphere of the SAPO-34 particles are already blocked, before organic deposits can be formed in the inner spheres. On the other hand, the weakly acidic terminal OH groups located at the outer surface of the SAPO-34 particles keep their accessibility for the reactant methanol, which is converted, in this situation, with high selectivity to DME (see Figure 3 for large TOS).

4. CONCLUSIONS

In the present work, SAPO-34 materials with comparable Brønsted acid site densities, but different crystal sizes (2.5 μm (SAPO-34-S), 6.0 μm (SAPO-34-M), and 20.0 μm (SAPO-34-L)) were prepared and applied as catalysts in the MTO conversion. Catalytic investigations demonstrated that the lifetime of the above-mentioned SAPO-34 catalysts in the MTO reaction strongly depend on the crystal size: SAPO-34-S > SAPO-34-M > SAPO-34-L. Thermographimetric analysis indicated that the deactivation of the SAPO-34 catalysts under study is accompanied by the formation of coke deposits. For elucidating the mechanism of this catalyst deactivation, ^{13}C HPDEC MAS NMR, FTIR, and UV/vis spectroscopy were employed to monitor the formation and nature of organic deposits during the MTO conversion. By ^{1}H MAS NMR spectroscopy, the nature and density of accessible Brønsted acid sites and active hydrocarbon-pool species were determined as a function of the time-on-stream (TOS).

The picture of the deactivation mechanism obtained by the above-mentioned spectroscopic methods was found to be very complex and consists of the following elements:

(i) Already in the active period of the catalyst lifetime, a rapid and strong decrease of the density of accessible Brønsted acid sites occurs, while the number of benzene-base carbenium ions increases (^{1}H MAS NMR).
(ii) The appearance of benzene-based carbenium ions is accompanied by the formation of alkyl aromatics (UV/vis).
(iii) More pronounced for SAPO-34 catalysts with large crystal sizes and longer reaction time, these alkyl aromatics have longer alkyl chains with methylene carbon atoms (^{13}C HPDEC MAS NMR), which improve at first the selectivity to light olefins, but also hinder the diffusivity of reaction products for longer reaction times.
(iv) Simultaneously with the formation of large alkyl aromatics, olefinic reaction products with enhanced residence time inside the SAPO-34 cages and pore were observed (FTIR).
(v) Because of the high reactivity of the olefinic reaction products with enhanced residence time, the formation of polycyclic aromatics occurs (UV/vis), which causes a blocking of the catalyst pores.
(vi) Finally, because of the pore blocking by the large aromatic deposits, neither Brønsted acid sites nor catalytically active carbenium ions are accessible for further reactants (^{1}H MAS NMR). This leads to a strong decrease in the olefin formation over the SAPO-34 materials in the MTO reaction. In this situation, methanol is preferentially converted to DME at terminal OH groups located at the outer surface of the zeolite particles.

Because of the high significance of the reactant diffusion for the last steps of the above-mentioned deactivation mechanism, the total deactivation of the large-crystalline SAPO-34-L material studied in the present work occurred after a much shorter MTO reaction time and is much more rapid than observed for SAPO-34-S and SAPO-34-M with significantly smaller crystal sizes.

dx.doi.org/10.1021/cs400007v | ACS Catal. 2013, 3, 588−596

■ ASSOCIATED CONTENT

Supporting Information

Additional information as noted in text. This material is available free of charge via the Internet at http://pubs.acs.org.

■ AUTHOR INFORMATION

Corresponding Author

*(M.H.) Fax: +49-711-685-64081. E-mail: michael.hunger@itc.uni-stuttgart.de. (L.L.) Fax: +86-22-2350-0341. E-mail: lild@nankai.edu.cn.

Notes

The authors declare no competing financial interest.

■ ACKNOWLEDGMENTS

This work was supported by the National Basic Research Program of China (2009CB623502), 111 Project (B12015), and the Ministry of Education of China (NCET-11-0251). M.H. is grateful for for financial support by Fonds der Chemischen Industrie and Deutsche Forschungsgemeinschaft.

■ REFERENCES

(1) Stöcker, M. *Microporous Mesoporous Mater.* **1999**, *29*, 3−48.
(2) Chen, J. Q.; Bozzano, A.; Glover, B.; Fuglerud, T.; Kvisle, S. *Catal. Today* **2005**, *106*, 103−107.
(3) White, J. L. *Catal. Sci. Technol.* **2011**, *1*, 1630−1635.
(4) Ilias, S.; Bhan, A. *ACS Catal.* **2013**, *3*, 18−31.
(5) Olsbye, U.; Svelle, S.; Bjørgen, M.; Beato, P.; Janssens, T. V. W.; Joensen, F.; Bordiga, S.; Lillerud, K. P. *Angew. Chem., Int. Ed.* **2012**, *51*, 5810−5831.
(6) Djieugoue, M. A.; Prakash, A. M.; Kevan, L. *J. Phys. Chem. B* **2000**, *104*, 6452−6461.
(7) Zhu, Z.; Hartmann, M.; Kevan, L. *Chem. Mater.* **2000**, *12*, 2781−2787.
(8) Svelle, S.; Olsbye, U.; Joensen, F.; Bjørgen, M. *J. Phys. Chem. C* **2007**, *111*, 17981−17984.
(9) Park, J. W.; Kim, S. J.; Seo, M.; Kim, S. Y.; Sugi, Y.; Seo, G. *Appl. Catal., A* **2008**, *349*, 76−85.
(10) Castro, M.; Warrender, S. J.; Wright, P. A.; Apperley, D. C.; Belmabkhout, Y.; Pirngruber, G.; Min, H. K.; Park, M. B.; Hong, S. B. *J. Phys. Chem. C* **2009**, *113*, 15731−15741.
(11) Lee, J. H.; Park, M. B.; Lee, J. K.; Min, H. K.; Song, M. K.; Hong, S. B. *J. Am. Chem. Soc.* **2010**, *132*, 12971−12982.
(12) Dai, W. L.; Wang, X.; Wu, G. J.; Guan, N. J.; Hunger, M.; Li, L. D. *ACS Catal.* **2011**, *1*, 292−299.
(13) Li, J.; Wei, Y. X.; Liu, G.; Qi, Y.; Tian, P.; Li, B.; He, Y.; Liu, Z. *Catal. Today* **2011**, *117*, 221−228.
(14) Wang, Q.; Cui, Z. M.; Cao, C. Y.; Song, W. G. *J. Phys. Chem. C* **2011**, *115*, 24987−24992.
(15) Li, J. Z.; Wei, Y. X.; Chen, J. R.; Tian, P.; Su, X.; Xu, S. T.; Qi, Y.; Wang, Q. Y.; Zhou, Y.; He, Y. L.; Liu, Z. M. *J. Am. Chem. Soc.* **2012**, *134*, 836−839.
(16) Teketel, S.; Skistad, W.; Benard, S.; Olsbye, U.; Lillerud, K. P.; Beato, P.; Svelle, S. *ACS Catal.* **2012**, *2*, 26−37.
(17) Bhawe, Y.; Moliner-Marin, M.; Lunn, J. D.; Liu, Y.; Malek, A.; Davis, M. *ACS Catal.* **2012**, *2*, 2490−2495.
(18) Hereijgers, B. P. C.; Bleken, F.; Nilsen, H. M.; Svelle, S.; Lillerud, K.-P.; Bjørgen, M.; Weckhuysen, B. M.; Olsbye, U. *J. Catal.* **2009**, *264*, 77−87.
(19) Olsbye, U.; Bjørgen, M.; Svelle, S.; Lillerud, K. P.; Kolboe, S. *Catal. Today* **2005**, *106*, 108−111.
(20) Guisnet, M. *J. Mol. Catal. A* **2002**, *182*−*183*, 367−382.
(21) Qi, G. Z.; Xie, Z. K.; Yang, W. M.; Zhong, S. Q.; Liu, H. X.; Zhang, C. F.; Chen, Q. L. *Fuel Process. Technol.* **2007**, *88*, 437−441.
(22) Van Niekerk, M. J.; Fletcher, J. C. Q.; O'Connor, C. T. *Appl. Catal., A* **1996**, *138*, 135−145.
(23) Mees, F. D. P.; Van Der Voort, P.; Cool, P.; Martens, L. R. M.; Janssen, M. J. G.; Verberckmoes, A. A.; Kennedy, G. J.; Hall, R. B.; Wang, K.; Vansant, E. F. *J. Phys. Chem. B* **2003**, *107*, 3161−3167.
(24) Bleken, F.; Bjørgen, M.; Palumbo, L.; Bordiga, S.; Svelle, S.; Lillerud, K.-P.; Olsbye, U. *Top. Catal.* **2009**, *52*, 218−228.
(25) Dai, W. L.; Wang, X.; Wu, G. J.; Li, L. D.; Guan, N. J.; Hunger, M. *ChemCatChem* **2012**, *4*, 1428−1435.
(26) Chen, D.; Moljord, K.; Fuglerud, T.; Holmen, A. *Microporous Mesoporous Mater.* **1999**, *29*, 191−203.
(27) Lee, Y. J.; Baek, S. C.; Jun, K. W. *Appl. Catal., A* **2007**, *329*, 130−136.
(28) Lee, K. Y.; Chae, H.-J.; Jeong, S.-Y; Seo, G. *Appl. Catal., A* **2009**, *369*, 60−66.
(29) Nishiyama, N.; Kawaguchi, M.; Hirota, Y.; Vu, D. V.; Egashira, Y.; Ueyama, K. *Appl. Catal., A* **2009**, *362*, 193−199.
(30) Wang, P. F.; Lv, A. L.; Hu, J.; Xu, J. A.; Lu, G. Z. *Microporous Mesoporous Mater.* **2012**, *152*, 178−184.
(31) Tan, J.; Liu, Z. M.; Bao, X. H.; Liu, X. C.; Han, X. W.; He, C. Q.; Zhai, R. S. *Microporous Mesoporous Mater.* **2002**, *53*, 97−108.
(32) Iwase, Y.; Motokura, K.; Koyama, T.-R.; Miyaji, A.; Baba, T. *Phys. Chem. Chem. Phys.* **2009**, *11*, 9268−9277.
(33) *Collection of Simulated XRD Powder Patterns for Zeolites*, 5th revised ed.; Treacy, M. M. J., Higgins, J. B., Eds.; Elsevier: Amsterdam; 2007.
(34) Hunger, M.; Brunner, E. In *Molecular Sieves − Science and Technology*, Karge, H. G., Weitkamp, J., Eds.; Springer-Verlag: Berlin, 2004; Vol. *4*; pp 201−293.
(35) Buchholz, A.; Wang, W.; Xu, M.; Arnold, A.; Hunger, M. *Microporous Mesoporous Mater.* **2003**, *57*, 157−168.
(36) Zibrowius, B.; Loeffler, E.; Hunger, M. *Zeolites* **1992**, *12*, 167−174.
(37) *Spektroskopische Methoden in der organischen Chemie*, 8th revised ed.; Hesse, M., Meier, H., Zeeh, B.; Georg Thieme Verlag: Stuttgart, 2011; pp 232−234.
(38) Hunger, M. *Microporous Mesoporous Mater.* **2005**, *82*, 241−255.
(39) Petkovic, L. M.; Ginosar, D. M.; Burch, K. C. *J. Catal.* **2005**, *234*, 328−339.
(40) Bjørgen, M.; Bonino, F.; Arstad, B.; Kolboe, S.; Lillerud, K.-P.; Zecchina, A.; Bordiga, S. *ChemPhysChem* **2005**, *6*, 232−235.
(41) Park, J. W.; Seo, G. *Appl. Catal., A* **2009**, *356*, 180−188.
(42) Binder, H.; Anikin, A.; Kohlstrunk, B. *J. Phys. Chem. B* **1999**, *103*, 450−460.
(43) Dai, W. L.; Scheibe, M.; Guan, N. J.; Li, L. D.; Hunger, M. *ChemCatChem* **2011**, *3*, 1130−1133.
(44) Dai, W. L.; Scheibe, M.; Li, L. D.; Guan, N. J.; Hunger, M. *J. Phys. Chem. C* **2012**, *116*, 2469−2476.
(45) Jiang, Y.; Huang, J.; Reddy Marthala, V. R.; Ooi, Y. S.; Weitkamp, J.; Hunger, M. *Microporous Mesoporous Mater.* **2007**, *105*, 132−139.
(46) Kirisci, I.; Førster, H.; Tasi, G.; Nagy, J. B. *Chem. Rev.* **1999**, *99*, 2085−2114.
(47) Bjørgen, M.; Bonino, F.; Kolboe, S.; Lillerud, K.-P.; Zecchina, A.; Bordiga, S. *J. Am. Chem. Soc.* **2003**, *125*, 15863−15868.
(48) Karge, H. G.; Laniecki, M.; Ziolek, M.; Onyestyak, G.; Kiss, A.; Kleinschmit, P.; Siray, M. In *Zeolites: Facts, Figures, Future*;8th International Zeolite Conference; Amsterdam, Netherlands; 1989; Studies in Surface Science and Catalysis; Jacobs, P. A., van Santen, R. A., Eds.; Elsevier: Amsterdam, 1989; Vol. *49*; p 1327.
(49) Mohan, J. *Organic Spectroscopy Principles and Applications*; Alpha Science International Ltd.: Harrow, 2002; pp 128, 137.
(50) Park, J. W.; Lee, J. Y.; Kim, K. S.; Hong, S. B.; Seo, G. *Appl. Catal., A* **2008**, *339*, 36−44.